Using the Galileo Solid-State Imaging Instrument as a Sensor of Jovian Energetic Electrons

Ashley Carlton[1], Maria de Soria-Santacruz Pich[2], Insoo Jun[2], Wousik Kim[2], and Kerri Cahoy[1]

[1]Massachusetts Institute of Technology, Cambridge, 02139, USA (e-mail: acarlton@mit.edu)
[2]Jet Propulsion Laboratory, California Institute of Technology, Pasadena, 91109, USA

I. Introduction

Harsh radiation in the form of ionized, highly energetic particles is part of the space environment and can affect spacecraft. These particles not only sweep through the solar system in the solar wind and flares and are ejected from galactic and extra-galactic supernovae, but also are trapped as belts in planetary magnetic fields. Jupiter's magnetosphere is the largest and strongest of a planet in the solar system. Similar to Earth, Jupiter is roughly a magnetic dipole with a tilt of ~11° [Khurana et al., 2004]. Jupiter's magnetic field strength is an order of magnitude larger than Earth, and its magnetic moment is roughly 18,000 times larger [Bagenal et al., 2004]. The Jupiter magnetosphere is powered by a liquid dynamo circulating metallic hydrogen. Eruptions of sulfur and oxygen from the moon Io's volcanoes form a cold torus that rotates with Jupiter, generating ions through collisions and ultraviolet radiation, altering the dynamics of and supplying the mass to the magnetosphere [Johnson and Soderblom, 1981; Krupp et al., 2004]. The Jovian radiation environment is dominated by trapped high-energy electrons, which can cause increased radiation dose damage and risk of internal electrostatic discharge [Frederickson, 1996]. The high-energy electron spectrum extends to much higher energies (>10 MeV) than the spectra found near Earth [Bolton et al., 1992; Garrett et al., 2005; de Soria-Santacruz Pich et al., 2016].

Determining the composition of energetic particles is fundamental to understanding the energetic processes powering the magnetosphere for studying interactions with the satellites (and rings and upper atmosphere) of Jupiter and the effects on spacecraft in orbit near or around Jupiter. The energetic electrons are a major contributor to exogenic processes that affect the albedo and surface chemistry of the moon [Chyba and Phillips, 2001; Marion et al., 2003]. MeV electrons can penetrate through atmospheres, physically and chemically weathering the surfaces of satellites. Spacecraft operating in high-energy radiation environments can experience component failures, degradation of sensors and solar panels, and serious physical damage to materials [Hastings and Garrett, 1996; and references therein]. Secondary particles from high-energy electron interactions produce transients and background noise in detectors and sensors. The greatest risks come from radiation dose, which is a concern with electrons from 100 keV to 50 MeV. We work to detect and characterize the higher energy (>1 MeV) part of the range.

Measurements of the high-energy (>1 MeV) electron environment at Jupiter are currently spatially and temporally limited. Pioneers 10 & 11 and Voyagers 1 & 2 made measurements during flybys in the 1970s and 1980s, respectively. For the most part, information about the Jovian environment comes from the Galileo spacecraft Energetic Particle Detector (EPD) [Williams et al., 1992] (in Jovian orbit from December 1995 to September 2003), which had a nearly equatorial orbit. Juno, a NASA spacecraft that entered Jovian orbit in July 2016, and Europa Clipper, a NASA mission planned for the 2020s, do not carry instruments capable of measuring high-energy (>1 MeV) electrons. Juno is in a polar orbit; Europa Clipper is planned to be in a highly elliptical Jovian orbit, flying-by Jupiter's moon, Europa, in each orbit.

We develop a technique to extract the high-energy electron environment using scientific imager data. Imagers are common to spacecraft and are sensitive to MeV radiation [Daud et al., 1987; Janesick, 2001]. On the Juno spacecraft, there is an Ultraviolet Spectrograph (UVS) as well as three charge-coupled devices (CCDs): the Juno Color Camera (JunoCAM), the Advanced Stellar Compass (ASC), and the Stellar Reference Unit (SRU). On Europa Clipper, there are four planned imaging instruments: the Ultraviolet Spectrograph (UVS), the Mapping Imager Spectrometer for Europa (MISE), the Europa Imaging System (EIS), and the Mass SPectrometer for Planetary EXploration (MASPEX). Each instrument presents an opportunity to extract science information about the environment.

II. Approach

A. Overview

We develop a technique to extract environment information from a science imager using the Galileo Solid-

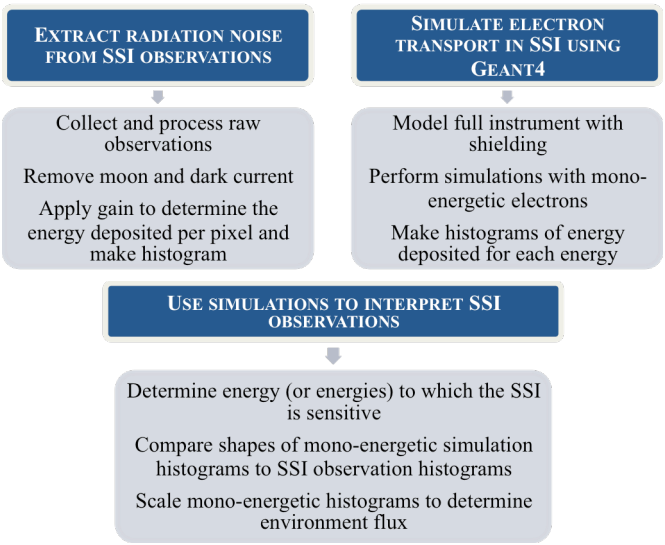

Figure 1. Diagram of the technique for extracting high-energy electron information from the Galileo Solid-State Imaging (SSI) flight data.

State Imaging (SSI) experiment, an overview of which can be found in Fig. 1. We determine the energy (or energies) that the imager is sensitive to and the environment flux at that energy. We use particle transport code (Geant4) to model the passage of electrons through the instrument to the detector. The number of pixels with hits and the energy deposited in those hits are used to scale back to the simulation environment. For the energy measurement, the goal is to extract a range of energies or an integral energy channel that the imager is sensitive to. For a science instrument, which is typically well-shielded, we expect to detect higher energies (>1 MeV). For the flux, we calculate geometric factors from the simulations that can then be applied to the pixels with hits on the imager.

B. Experiment: SSI Flight Data

The SSI experiment is a high-resolution (1500 mm focal length) system with a spectral range of approximately 375 to 1100 nm. The detector is an 800 by 800 pixel virtual-phase, silicon charge-coupled device (CCD). The dimensions of the detector are 12.19 x 12.19 mm with a 65.6 pixel per millimeter pixel density. For more details on the camera system, detector response, and early in-flight performance, see [Belton et al., 1992; Klaasen et al., 1997], and references therein.

We collect the raw SSI images and their associated calibration files (dark current, radiometric calibration, blemish, and shutter offset files) from the Planetary Data System (PDS). Due to an anomaly with the Galileo high-gain antenna [Johnson, 1994], a majority of the images were compressed with loss of information. We select the images that have not undergone lossy compression or spike reduction on-board, leaving only 767 out of a total of 4002 images (19%) for evaluation in this study.

We process the flight data, subtracting the dark current from the imager data and applying the calibrated instrument gain. The digital number (DN) ranges from 0 to 255 and the instrument gain converts the DN to electrons. There are four gain states; their factors can be found in Table I. For silicon, the ionization energy needed to create an electron-hole pair is 3.6 electron-Volts [Scholze et al., 1998]. The processed image is a matrix of energy deposited in each pixel, which can then be binned to form a histogram of energy deposited by the number of pixels.

Fig. 2 shows an SSI observation of Europa, one of Jupiter's moons. Fig. 3 shows the DN as the distance from the center of the moon increases (in pixels). While some of the high-DN (greater than DN=120) pixels between 0 and 95 pixels from the center of the moon are likely radiation, all pixels in this region

TABLE I. GAIN STATES FOR CONVERTING DIGITAL NUMBER TO ELECTRONS. GAIN STATE RATIO FACTORS ARE FOUND IN THE CALIBRATION FILES. UNCERTAINTIES FROM THE ORIGNAL CALIBRATION CAN BE FOUND IN THE JPL CALIBRATION REPORT [KLAASEN, 1993]

Commanded Gain	*Gain State Ratio Factors*	*Conversion [e-/DN]*	*Notes*
0 = Gain 1	1.00	1822	Summation mode only, ~400 K full scale
1 = Gain 2	4.824	377.4	Low gain, ~100 K full scale
2 = Gain 3	9.771	186.5	~40 K full scale
3 = Gain 4	47.135	38.66	High gain, ~10 K full 255 DN scale

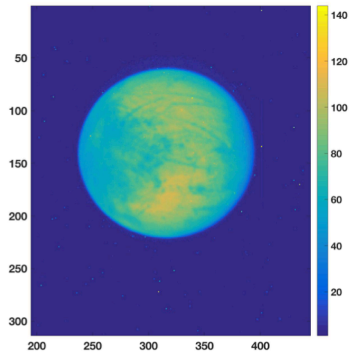

Figure 2. Galileo SSI image of Europa. The image was taken in a 240 by 300 pixel window of the 800 by 800 pixel arryay. The image was taken at 17.7 R_J (L-shell of 17.0). The intensity scale is in digital number (DN).

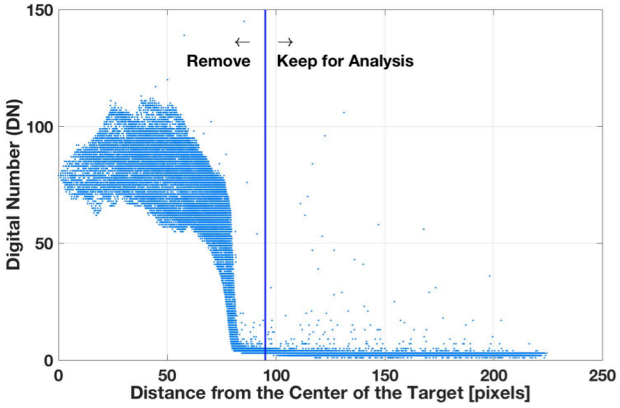

Figure 3. Digital number (DN) as a function of distance from the center of the moon. The vertical line is drawn at 95 pixels from the center of the moon, dividing the moon from the dark sky for the analysis.

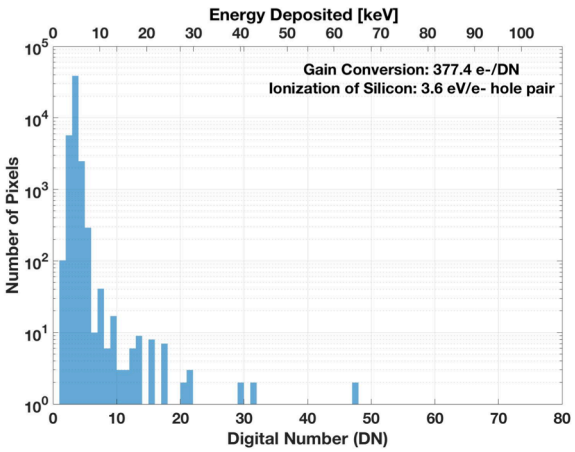

Figure 4. Histogram of the energy deposited in the moon-removed image. The lower x-axis is the digital number and the upper x-axis labels the corresponding energy deposited in kiloelectron-Volts.

are excluded at present, because radiation hits here are not distinguishable from photons reflected by the moon. A histogram of the number of pixels with a given DN is plotted in Fig. 4. The energy deposited in kiloelectron-Volts (keV) is also provided.

C. Simulations in Geant4

We simulate electron transport in the SSI to determine the energies of the source particles that can reach the detector (in the form of pixels with hits) and the amount of energy that is deposited in the pixels. We use a Monte Carlo particle transport code called Geant4 [Agostinelli et al., 2003]. Particles are tracked from the source environment to the target (the detector, in this case). Geant4 is capable of modeling all particles relevant to the space environment (electrons, photons, protons, neutrons, and heavy ions).

We model the SSI instrument in three dimensions, a cut-away visualization of which is shown in Fig. 5 with labels of the key components. Both the materials and physical placements are accounted for in the geometry. We perform mono-energetic electron runs in Geant4 for energies of 1, 3, 5, 10, 30, 50, 100, and 200 MeV with one billion electrons. The source environment is an isotropic sphere with a radius of 150 centimeters radiating inward towards the detector, which is located at the center of the sphere. For a simulation of $1x10^9$ electrons at each energy, we calculate the number of pixels with energy deposited in them. Table II gives the results for those simulations. For each energy, the number of unique primary and secondary particles and the number of pixels with energy deposited in the 800 by 800 pixel array are recorded. Secondary particles are any order (2nd, 3rd, etc.) particles that are not primary particles.

For each of the mono-energetic simulations, we build a histogram of the energy deposited in the detector. Fig. 6 plots the histograms of energy deposited by energy. We try to identify distinctive shapes of the mono-energetic histograms, in which case the fitted curves would be used as a basis function and fit to the SSI energy histograms. In other words, for each energy, the multiplicative factor for the curve to match the SSI

TABLE II. RESULTS OF GEANT4 SIMULATIONS FOR PARTICLES THAT REACH THE SSI DETECTOR AND DEPOSIT ENERGY. THE GEANT4 SIMULATIONS ARE OF 1E9 ELECTRONS WITH ENERGIES 1, 3, 5, 10, 30, 50, 100, AND 200 MEV. COLUMNS B AND C ARE THE NUMBERS OF UNIQUE PRIMARY AND SECONDARY PARTICLES THAT DEPOSIT ENERGY ON THE DETECTOR, RESPECTIVELY, AND THEIR SUM IS IN COLUMN D. COLUMN E IS THE TOTAL NUMBER OF PIXELS WITH ENERGY DEPOSITION ("HITS") AND COLUMN F IS THE RATIO OF PARTICLE HITS TO PIXEL HITS (COLUMN D DIVIDED BY COLUMN E).

A	*B*	*C*	*D*	*E*	*F*
Energy [MeV]	*# Unique Hits*			*# Pixels with Hits*	*Particle to Pixel Hits (D/E)*
	Primaries	*Secondaries*	*Total (B+C)*		
1	0	0	0	0	n/a
3	0	6	6	11	0.53
5	1	19	20	57	0.35
10	37	91	128	241	0.53
30	329	1063	1392	2529	0.53
50	626	2544	3170	5910	0.54
100	1197	8063	9260	17742	0.52
200	1975	20573	22548	44281	0.51

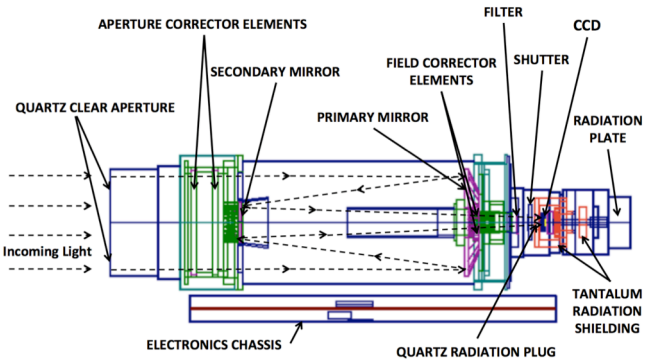

Figure 5. Cut-away visualization of the geometry built in Geant4 of the SSI. The key components are labeled. The colors correspond to the material of the element (yellow - silicon, dark blue - aluminum, cyan - titanium, green - invar, pink - silica, red orange - tantalum, brown - printed wiring board).

histograms would translate to the flux for the given energy. If energy deposition curves do not have a distinct shape, we will extract an integral flux. The next steps include performing more simulations (5 to 10 per energy) to be able to place a confidence interval on the energy range for detection and the number of particles of a given energy that reach the detector.

III. RESULTS

A. Energy Measurement

The mono-energetic simulations of 1, 3, and 5 MeV deposit little or no energy on the detector; fewer than 0.009% of pixels are hit for the 5 MeV case. The detection energy for the detector is in the >10 to >50 MeV range. The minimum equivalent shielding of Aluminum for the detector is ~25 mm (or 1000 mils). This corresponds to a dose depth penetration for electrons of ~10 MeV, which is consistent with the simulation findings. Future work for this case study includes refining the cut-off energy and placing a confidence interval on the number.

Looking at Fig. 6, the shapes of the energy deposition curves for 30 to 200 MeV are similar. In order to better understand why these curves look similar, we plot the energy deposited on the detector as a function of the kinetic energy of the particles at the detector (see Fig. 7) and find the results are consistent with the stopping power of electrons in silicon.

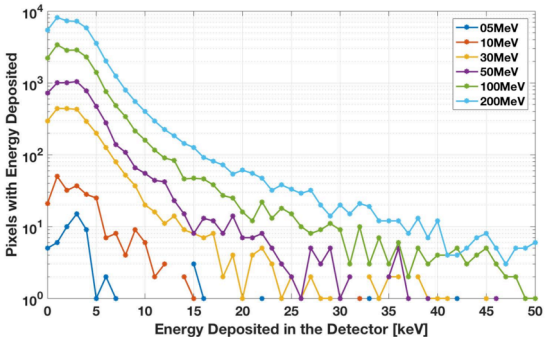

Figure 6. Histograms of the energy deposited from the Geant4 simulations of 5, 10, 30, 50, 100, and 200 MeV electrons. The data has a bin width of 1 keV.

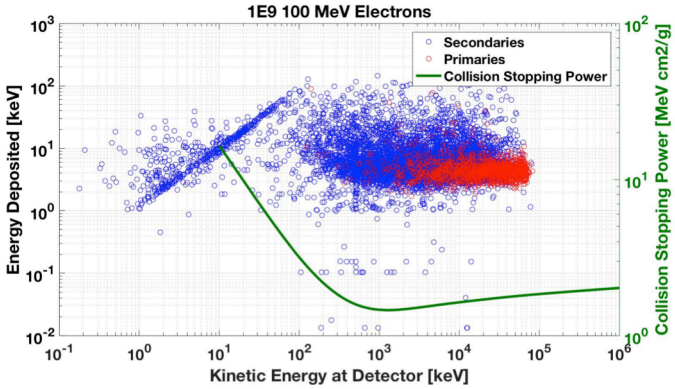

Figure 7. Energy deposited in the detector (left y-axis) as a function of the energy of the particle at the detector for 100 MeV electrons. The primary particles are red circles and the secondaries are blue circles. The collision stopping power is plotted in green on the right y-axis.

From about 1 to 80 keV, there is roughly a one-to-one ratio between the energy at the detector and the energy deposited. This is because the majority of the lower-energy particles are depositing all of their energy on the detector. For a kinetic energy of >100 keV at the detector, the incident energy does not affect the energy deposited. From about 10^{-1} to 10^{2} MeV, the stopping power is roughly flat, indicating roughly the same stopping power (MeV cm^2/g) for the energy range. The continuous-slowing-down approximation (CSDA) range for 90 keV electrons is ~0.4734 grams per square centimeter [ICRU, 1984]. Dividing by the density of silicon (2.33 grams per cubic centimeter), that gives an approximate thickness of silicon of 20 μm, which is very close to the 15 μm thickness of the detector's sensitive layer in the model, showing that the simulations are consistent with estimates.

B. *Flux Measurement*

The only information from the SSI flight data is the number of pixels with hits with certain digital numbers. We use the mono-energetic Geant4 simulations (since the flux was our input to Geant4) to determine the geometric factors. To convert the number of pixels with energy deposited to the flux in the environment, there are several steps, in terms of "geometric factors," which are a combination of efficiencies and the physical view factor of the detector. The number of particles that reach the detector and deposit energy depends on: the energy of the source particles, the number of source particles, the surface area of the source sphere (in 4π space), the shielding materials (response to energetic particles, *i.e.,* generation of secondaries) and geometry (thickness), the surface area of the detector, and other detector properties.

Referring to the mono-energetic simulation results in Table II, from the total number of pixels with energy deposited (column E), we calculate the ratio of particles to pixels with hits G_1 (column F). The pixel count rate is R_0 and the particle count rate is R_1, scaled by G_1, using the following equation:

$$R_1 = R_0 G_1 \tag{1}$$

From Table II, ignoring 1, 3, and 5 MeV, there is a common factor of $G_1 = 0.53 \pm 0.014$ (95% confidence) relating the number of pixels to the number of particles. This factor will be different for a given instrument, and must be calculated through analysis of charged particle transport simulations, as shown here.

For the Geant4 simulations, we know the input flux: $N = 1 \times 10^9$ source electrons, coming from a 4π sphere of radius $r = 150$ square centimeters, so we can write the particle flux f_0 from the simulation as:

$$f_0 = \frac{N}{4\pi(4\pi r^2)} = \frac{1\times10^9}{4\pi(4\pi(150cm)^2)} \tag{2}$$

To represent the real environment, f_0 needs to multiplied by four: a factor of two because the simulation is a sphere with particles going in (real environment is in and out), and another factor of two because the simulation is a cosine distribution (the real environment is isotropic). Since we know the flux f_0 of the mono-energetic simulations and the converted count rate per unit area R_1 for each energy, we can calculate the second scale factor G_2, which will also be a function of energy E. G_2 has units of steradian.

$$R_1 = f_0 G_2(E) \tag{3}$$

$$G_2 = \frac{R_1}{f_0} \tag{4}$$

For each pixel count rate in the mono-energetic Geant4 simulations (see Table II), we calculate the scale factors, $G_2(E)$, which are listed in Table III.

C. *Analysis of an SSI Image: 5101r, orbit 22*

As an example, we select an image taken in orbit 22 (1999-08-12T19:13:10.828z) at 9.4 R_J of Amalthea. After Amalthea is identified, removed, and the dark current is subtracted, we find 295 out of 4161 pixels with hits (7.09%). The integration time is 62.5 milliseconds and the readout time is 8.667 seconds (the shutter contributes very little to blocking the high-energy electrons, so we include the readout time). The pixel hit rate per unit area R_0 over the image is:

$$R_0 = \frac{295px}{4161px} \times \frac{1px}{(15\mu m)^2} \times \frac{1}{0.0625s + 8.667s} = 3610 \frac{px}{cm^2 s} \tag{5}$$

Converting (5) to the particle rate per unit area, using $G_1 = 0.53$ and (1),

$$R_1 = (3610)(0.53) = 1913 \frac{\#}{cm^2 s} \tag{6}$$

TABLE III. GEOMETRIC SCALE FACTOR G_2 THAT RELATES THE PARTICLE COUNT RATE AT THE DETECTOR TO THE ENVIRONMENTAL FLUX FOR A GIVEN ENERGY.

Energy [MeV]	*Geometric scale factor, G_2 [sr]*
5	0.0036
10	0.0186
30	0.827
50	1.93
100	5.80
200	14.5

This particle count rate per unit area, R_1, is from particles in the environment from all energies (above a certain threshold, around 10 MeV and greater). Using G_2 in Table III and (4), we calculate the flux assuming all particles are from 10 MeV source particles: $f = 2.43 \times 10^4$ [cm^2-s-sr]$^{-1}$. This places an upper limit on the flux since some of the particles will be from higher and lower energies and will not contribute to the 10 MeV flux.

There is not a corresponding EPD measurement at the time of the observation, so we identify the average integral flux for the same distance ($R_J = 9.4$) and the same spacecraft latitude (0.633°). The EPD DC3 flux (>11 MeV flux) is 2.6×10^5 [#/cm^2-s-sr]. This is consistent with the calculated approximate differential flux within an order of magnitude with the flux derived from the SSI observation.

IV. Discussion and Future Work

We present a technique to extract high-energy electron energy and flux information using the Galileo Solid-State Imaging (SSI) instrument. We extract radiation noise from SSI flight images and compare the count rates and energy deposited to mono-energetic simulations of the SSI in Geant4. We find that the instrument is capable of detecting ~>10 MeV electrons. We calculate the scaling factors necessary to back out the flux from the count rate. This approach could be applied to other sets of imaging data in energetic electron environments, such as from star trackers in geostationary Earth orbits or science imagers on exploratory spacecraft, like the Europa Clipper mission, which can increase the available environment data using existing hardware on spacecraft.

The next steps include processing the remainder of the SSI images and extracting the radiation noise. For each image (at a given distance from Jupiter), we will calculate the differential environmental flux using the technique described in this paper. We will compare the flux values to the Galileo EPD and models of the Jovian environment. We will also perform more mono-energetic electron simulations to place error bars on the geometric scale factors for the flux and to better determine the low energy cut-off of the detector.

Acknowledgment

Funding for A. Carlton's work is provided by a NASA Space Technology Research Fellowship (NNX16AM74H). We acknowledge Galileo SSI and EPD data obtained from the Johns Hopkins University Applied Physics Laboratory (JHU/APL) and available in the Planetary Data System (https://pds.nasa.gov/). We would like to thank Ken Klaasen, Herb Brenemen, and Cynthia Phillips for their assistance with understanding and processing the Galileo SSI data. We would like to thank Shawn Kang for providing the first version of the SSI model in Geant4.

References

Agostinelli, A. et al., "Geant4—a simulation toolkit," in Nuclear Instruments and Methods in Physics Research Section A: Accelerators, Spectrometers, Detectors, and Associated Equipment, vol. 506, no. 3, 2003, pp. 250-303.

Bagenal, F., T. Dowling, and W. McKinnon, eds. Jupiter: The Planet, Satellites and Magnetosphere. Cambridge Planetary Science. Cambridge University Press, 2004.

Belton, Michael S. et al., "The Galileo Solid-State Imaging experiment," in Space Science Reviews, vol. 60, no. 1, 1992, pp. 413-455.

Bolton, S. et al., "Ultra-relativistic electrons in Jupiter's radiation belts," in Nature, vol. 415, no. 6875, 2002, pp.987-991.

Chyba, C. and C. Phillips, "Possible ecosystems and the search for life on Europa," in Proceedings of the National Academyof Sciences of the United States of America, vol. 98, no. 3, 2001, pp. 801-804.

Daud, T., J. Janesick, K. Evans, and T. Elliot, "Charged-couple-device response to electron beam energies of less than 1 keV up to 20 keV," in Optical Engineering, vol. 26, no. 8, 1987.

de Soria-Santacruz Pich, M. et al., "An empirical model of the high-energy electron environment at Jupiter," in Journal of Geophysical Research: Space Physics, vol. 121, no. 10, 2016, pp. 9732-9743.

Frederickson, A., "Upsets related to spacecraft charging," in IEEE Transactions on Nuclear Science, vol. 23, no. 2, 1996, pp. 426-441.

Garrett, H. et al., "A revised model of Jupiter's inner electron belts: updating the Divine radiation model," in Geophysical Research Letters, vol. 32, no. 4, 2005.

Hastings, D. and H. Garrett, Spacecraft-Environment Interactions. Cambridge Atmospheric and Space Science Series. Cambridge, UK: Cambridge University Press, 1996.

International Commission on Radiation Units and Measurements, "Stopping powers for electrons and positrons," Tech. rep. ICRU Report 37, 1984.

Janesick, J., Scientific Charge-Coupled Devices. Vol. PM83, Bellingham, Washingon: SPIE Press, 2001.

Johnson, T. and L. Soderblom, "Volcanic eruptions on Io: implications for surface evolution and mass loss," in IAU Colloquium 57: Satellites of Jupiter, Ed. by D. Morrison, 1981, p. 634.

Johnson, Michael R., "The Galileo high gain antenna deployment anomaly," Tech. rep. N94-33319. Pasadena, CA: California Institute of Technology, Jet Propolsion Laboratory, 1994.

Khurana, K. et al., "The configuration of Jupiter's magnetosphere," in Jupiter: The Planet, Satellites and Magnetosphere," Ed. by F. Bagenal, T. Dowling, and W. McKinnon. Cambridge University Press, 2004. Chap. 24, pp. 559-616.

Krupp, N. et al., "Dynamics of the Jovian magnetosphere," in Jupiter: The Planet, Satellites and Magnetosphere," Ed. by F. Bagenal, T. Dowling, and W. McKinnon. Cambridge University Press, 2004. Chap. 25, pp. 617-638.

Klaasen, K., "Galileo solid-state imaging subsystem calibration report: part 2," JPL Document 1625-210. Pasadena, CA: California Institute of Technology, Jet Propolsion Laboratory, 1993.

Klaasen, K., M. Belton, H. Breneman, A. McEwen, M. Davies, and R. Sullivan, "Inflight performance characteristics, calibration, and utilization of the Galileo solid-state imaging camera," in Optical Engineerings, vol.36, no. 11, 1997, pp. 3001-3027.

Marion, G., C. Fritsen, H. Eicken, and M. Payne, "The search for life on Europa: limiting environmental factors, potential habitats, and Earth analogues," in Astrobiology, vol. 3, no. 4, 2003, pp. 785-811.

Scholze, F., H. Rabus, and G. Ulm, "Mean energy required to produce an electron-hole pair in silicon for photons of energies between 50 and 1500 eV," in Journal of Applied Physics, vol. 84, no. 5, 1998, pp. 2926-2939.

Williams, D., R. McEntire, S. Jaskulek, and B. Wilken, "The Galileo Energetic Particle Detector," in Space Science Reviews, vol. 60, 1992, pp. 385-412.